

THREE-DIMENSIONAL X-RAY IMAGING USING HYBRID DATA COLLECTED WITH A DIGITAL PANORAMIC DEVICE

1. INTRODUCTION

Three-dimensional X-ray imaging tools for implant planning include full-angle tomography using a dedicated dental CT device and limited-angle tomography using a panoramic device (reprogrammed to collect projection data using a scanning procedure). While the former produces comprehensive reconstructions of the tissue, the benefit of the latter option is lower radiation dose and the possibility to use cost-effective standard equipment. Three-dimensional reconstruction from limited-angle data using projection data from a scanning panoramic device is challenging; it is especially difficult to reconstruct edges perpendicular to the projection directions [5, 6]. However, such imaging is realized commercially in the VT product of PaloDEx Group and shown to yield clinically useful three-dimensional information [1, 3].

It is of course possible to use the panoramic device to take a standard panoramic image of a patient in addition to the scanned projection images. Furthermore, the direction of X-rays measured in the formation of is roughly perpendicular to the directions of the scanned projection radiographs. Thus we expect that combining panoramic and projection data in the reconstruction process yields improved three-dimensional information.

The aim of the paper is to compare three-dimensional reconstructions computed from projection data alone, and from hybrid data. We demonstrate these methods by examples based on simulated *in silico* data and measured *in vitro* data from the

point of view of implant planning. The results suggest that a three-dimensional reconstruction even from limited-angle projection data alone allows measuring precisely how deep one can drill without damaging the nerve. Further, reconstruction from the combination of projection and panoramic gives more accuracy for the estimation of the location of a slice along the dental arc.

2. MATERIALS AND METHODS

2.1. Structure of projection data. The projection data sets used in this work consist of eleven radiographs taken from limited angle of view of ± 21 degrees. See Figure 1 for illustration of the projection geometry. We remark that the two-dimensional projection radiographs are measured by moving the panoramic device in a special way allowing the narrow CCD sensor to scan the image.

We use the following linear measurement model for projection data:

$$m_1 = A_1 x,$$

where the vector x represents unknown voxel values in the tissue, vector m_1 contains all pixel values in the measured set of digital radiographs, and the matrix A_1 comes from the well-known pencil beam model of X-ray attenuation, see e.g. [6, 4].

2.2. Structure of panoramic data. The extension of tomosynthesis to a curved sharp layer is illustrated in Figure 2. As the panoramic X-ray device rotates around the patient's head, the CCD detector pixels behind the receiver are moved with such speed that the X-rays travelling through certain detail on the sharp layer are recorded at the same place on the digital image. This results in blurring of the details that do not lie on the sharp layer, but leaves the sharp layer itself accurate.

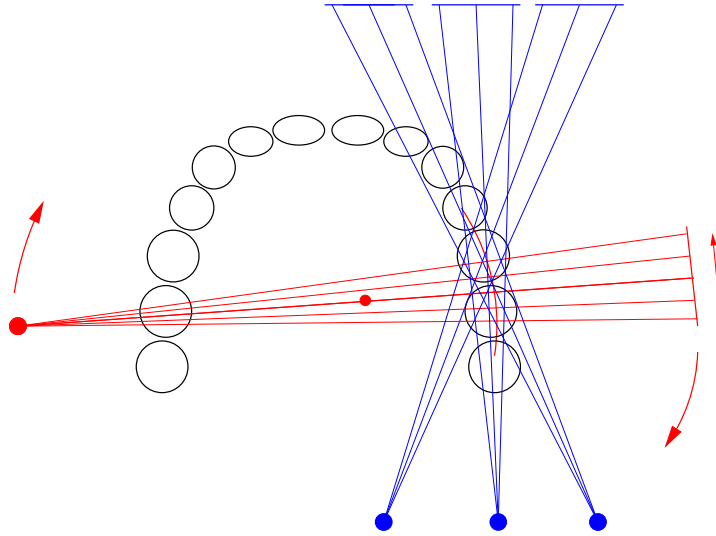


FIGURE 1. We collect two kinds of data. Projection data consists of a small number (less than a dozen) projections with directions roughly as shown by the blue lines. Panoramic data consists of the part of a panoramic image that shows the region of interest. The geometry of panoramic measurement is illustrated by the red lines.

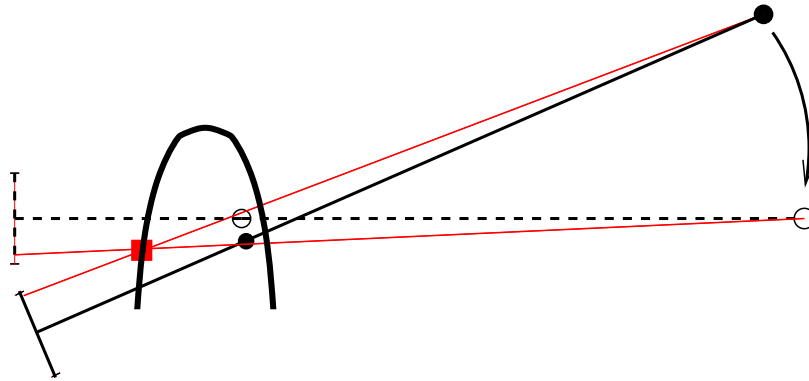


FIGURE 2. The generation of a panoramic image.

The value assigned to a point on the sharp layer can be interpreted as a sum of integrals of the absorption over multiple lines that pass through that particular

point. As a consequence, the panoramic image can be considered as the restriction of a suitable (unfiltered) back-projection reconstruction to the sharp layer.

We may approximate the panoramic image formation process by discretizing the movement of the panoramic X-ray device: assume that the device takes a divergent beam projection at some point in time, then rotates to a new position and moves the film accordingly, takes another projection, and so on. This way the panoramic image can be considered as a sum of overlapping *virtual* X-ray projections.

We use the following linear measurement model for panoramic data:

$$m_2 = A_2 x,$$

where the vector x represents unknown voxel values in the tissue, vector m_2 contains all pixel values in the part of the panoramic image we use, and the matrix A_2 comes from modifying the pencil beam model to cover the above approximation.

2.3. Test phantom and specimen. The simulated *in silico* phantom used in our experiments is illustrated in the top left image of Figure 3; it is a transversal slice of a CT reconstruction of a jaw specimen. It consists of 150×150 pixels that represent the absorption level of the phantom. We study the simulated phantom to be able to compare our reconstructions with a known ground truth. For simplicity we restrict to two-dimensional tomography; in case of the simulated phantom this is enough to demonstrate crucial features of our approach.

We perform experiments with an *in vitro* dry jaw specimen as well. This three-dimensional computation gives more realistic understanding about the suggested hybrid data imaging modality.

2.4. Regularized reconstruction method. All our experiment settings lead to the measurement model

$$(1) \quad m = Ax + \varepsilon,$$

where m is a vector containing the measured pixel values and the vector x is composed of the unknown voxel values. In the case of reconstruction from projection data only, we take $A = A_1$ and $m = m_1$ in (1). In the case of reconstruction from the combination of projection and panoramic data, we take

$$A = \begin{bmatrix} A_1 \\ A_2 \end{bmatrix} \quad \text{and} \quad m = \begin{bmatrix} m_1 \\ m_2 \end{bmatrix}$$

in (1). The vector ε represents random measurement error resulting from the photon counting process and electronic noise in the detector.

We reconstruct the attenuation coefficient values at the voxels using Tikhonov regularization [7] with derivative penalty:

$$(2) \quad \tilde{x} = \arg \min_x \{ \|Ax - m\|_2^2 + \alpha \|Lx\|_2^2 \},$$

where L is a discrete approximation of the Laplacian and α is the regularization parameter. In all our experiments, the minimization of the above functional is implemented with the conjugate gradient method [2].

3. RESULTS

3.1. Reconstruction of simulated phantom. The projection data of the simulated phantom consists of 11 simulated parallel beam projections from limited angle of view of ± 21 degrees with respect to the tangent of the sharp layer depicted by

the dashed line in the top left image of Figure 3. Each of the eleven simulated projections consist of the values of 200 parallel line integrals.

The used panoramic data corresponds to a limited angle of view of ± 5 degrees with respect to the normal of the sharp layer; this kind of opening angles are encountered in standard panoramic X-ray devices. The data is simulated by taking 20 parallel beam projections approximately along the normal of the sharp layer, computing the corresponding (unfiltered) backprojection image, and finally taking its restriction to the sharp layer. The panoramic radiograph is composed of 150 real numbers.

In order to avoid the inverse crime (unrealistically good reconstructions resulting from using the same discretization in both simulating data and computing reconstructions), the reconstructions are computed on a sparser 140×140 grid. We simulate measurement noise by contaminating both of our data sets by white noise of zero mean and standard deviation 0.02 times the maximum element of the data set in question.

Here, $A_1 \in \mathbb{R}^{n_1 \times N}$, $n_1 = 2200 = 11 \times 200$, $N = 19600 = 140 \times 140$, is the matrix that sends a vectorized 140×140 image onto the corresponding projection values. On the other hand, multiplication of a vectorized image by $A_2 \in \mathbb{R}^{n_2 \times N}$, $n_2 = 140$, produces the panoramic data. The matrix A_2 is constructed by taking the parallel beam projection matrix corresponding to the 20 directions almost parallel to the normal of the sharp layer, multiplying it from the left by its transpose, and finally deleting all rows that do not correspond to the 140 pixels on the sharp layer.

Further, $m_1 \in \mathbb{R}^{n_1}$ contains the noisy simulated projections values. The other part $m_2 \in \mathbb{R}^{n_2}$ is obtained by taking the noisy vector containing the 150 simulated

panoramic data values and interpolating it onto a sparser grid. The discrete approximation of the Laplacian appearing in (2) is constructed by using the standard five point mask.

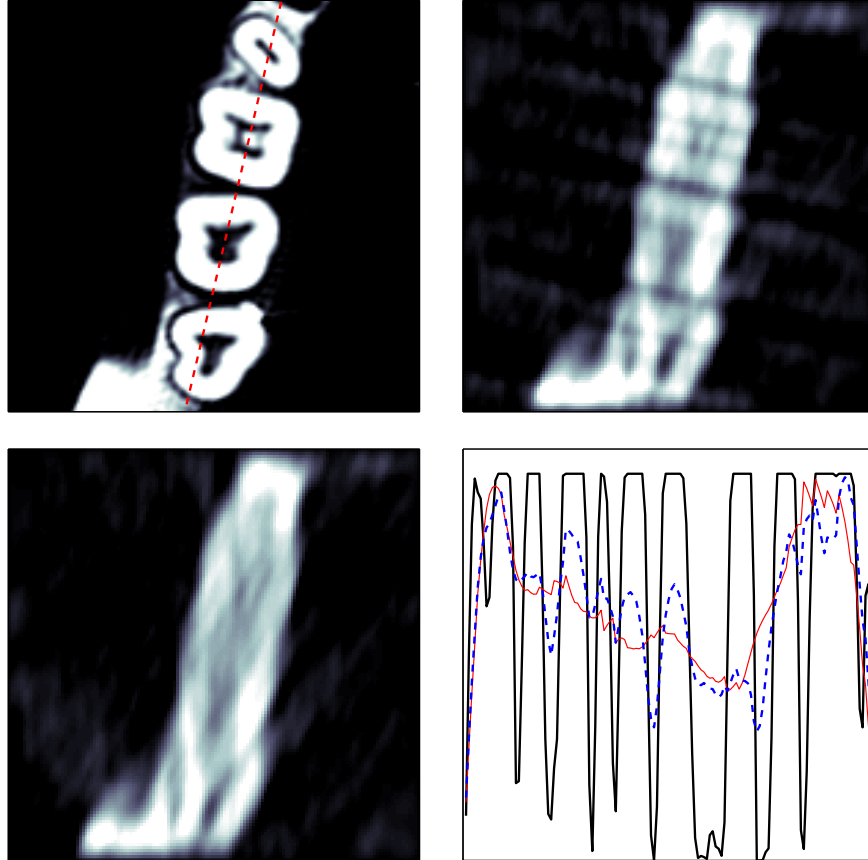


FIGURE 3. The reconstructions of the simulated phantom. Top left: The phantom. Top right: The reconstruction using both projection and panoramic data. Bottom left: The reconstruction using only projection data. Bottom right: The phantom (thick solid line), the top right reconstruction (dashed thick line), and the bottom left reconstruction (thin solid line) plotted along the sharp layer.

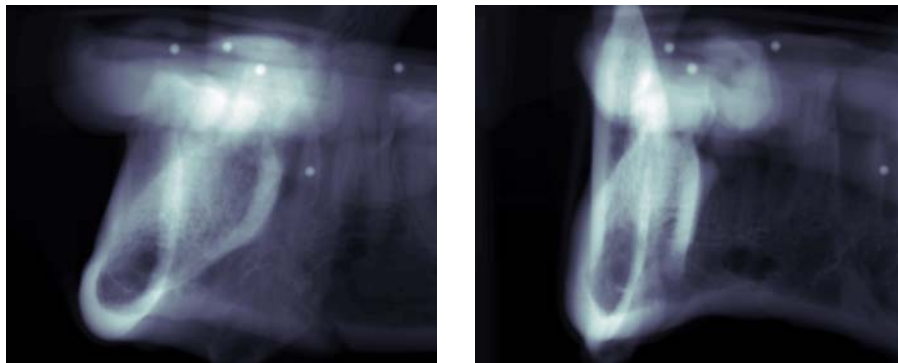


FIGURE 4. Two projection images of the *in vitro* jaw specimen.

In our computations, we used the value $\alpha = 0.01$ for the regularization parameter. The resulting reconstructions are illustrated in Figure 3, where the top left image depicts the original phantom, the top right image is the reconstruction obtained from both projection and panoramic data, and the bottom left image shows the reconstruction computed using the same parameter values but only the projection data.

3.2. Reconstruction from *in vitro* data. For the *in vitro* jaw specimen, the projection data consists of 11 divergent beam projections from limited angle of view of ± 21 degrees with respect to the left mandible. Two of the projections are shown in Figure 4.

The corresponding panoramic data set is illustrated in the right-hand image of Figure 5. It is constructed by taking a complete panoramic projection of the jaw specimen (the left-hand image of Figure 5), and then restricting the attention to the part that provides information on the ROI. By using our knowledge of the alignment of the panoramic X-ray device during the measurement process, the data image is interpreted as a sum of 100 virtual overlapping thin divergent beam

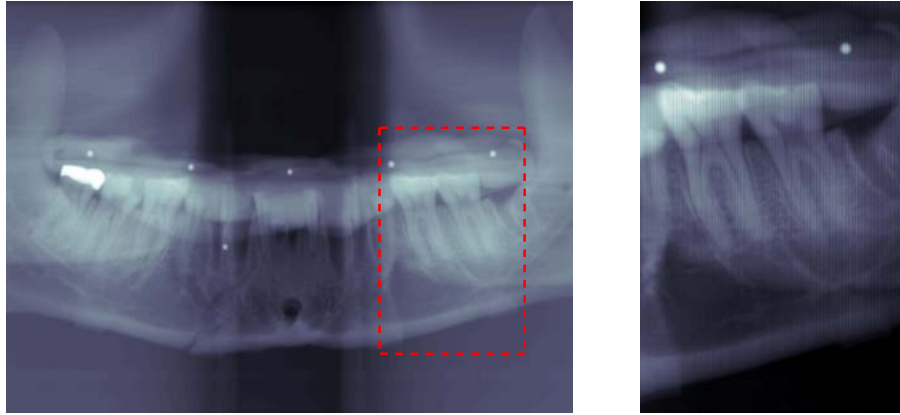


FIGURE 5. The panoramic images of the *in vitro* jaw specimen.

Left: The whole image with the ROI highlighted. Right: The ROI scaled so that it can be interpreted as a sum of multiple virtual projections.

projections taken at uniform time intervals; each pixel is typically treated as if it was obtained by summing ten pencil beam projections recorded at different positions of the measurement device. The pixel values are scaled in order to take into account the changes in the number of overlapping virtual projections. This explains the vertical stripes in the right-hand image of Figure 5.

When computing the reconstructions, the two data sets are aligned using the small metal pellets that are visible in Figures 4 and 5. What is more, the attenuation levels, i.e., the brightness, of the two data sets are matched by looking at certain well identifiable details in the corresponding X-ray images. Since this manual process cannot be considered very reliable, the mismatch between the two data sets is bound to cause some artefacts in the reconstructions. If our method is to be used in commercial panoramic X-ray devices, this step of alignment and fine-tuning of the pixel values must be automatized in order to obtain more reliable reconstructions.

To arrive at a computational model, the surroundings of the left mandible are divided into $230 \times 150 \times 200$ cubic voxels with the edge length 0.3mm. Here, the longest dimension corresponds approximately to the normal of the coronal plane, and the shortest one to the normal of the sagittal plane. Each of the eleven divergent beam projection images consists of 675×800 square pixels with edge length 0.096mm. The panoramic data set shown in the right-hand image is composed of 700×450 pixels of this same size.

Here, $A_1 \in \mathbb{R}^{n_1 \times N}$, $n_1 = 5940000 = 11 \times 675 \times 800$, $N = 6900000 = 230 \times 150 \times 200$, is the matrix that sends a vectorized $230 \times 150 \times 200$ voxel volume onto the corresponding eleven projection images. The second matrix A_2 can be written as

$$A_2 = \sum_{j=1}^{100} A_2^{(j)},$$

where $A_2^{(j)} \in \mathbb{R}^{n_2 \times N}$, $n_2 = 315000 = 700 \times 450$, is the projection matrix corresponding to the j th (discrete) position of the X-ray device during the measurement of the panoramic data. Because the device illuminates only about one tenth of the panoramic image depicted in the right-hand image of Figure 5 at one time, most rows of each $A_2^{(j)}$ are empty; since each pixel of the panoramic image can be treated as a sum of about ten virtual pencil beam projections, any particular row of A_2 is nonempty in about ten $A_2^{(j)}$.

Here, $m_1 \in \mathbb{R}^{n_1}$ contains the eleven vectorized projection images, and $m_2 \in \mathbb{R}^{n_2}$ is the vectorized panoramic image. The discrete approximation of the Laplacian appearing in (2) is constructed by using the standard seven point mask. Take note that the measurement matrix A is sparse but, anyway, so huge that it cannot be loaded into the memory in one part. Hence, the computations were conducted in a

matrix free way, i.e., the needed matrix multiplications were computed one row at a time.

In our computations, we used the value $\alpha = 0.2$ for the regularization parameter. The resulting three-dimensional reconstructions are presented in Figure 6, which illustrates a $128 \times 128 \times 128$ subvolume around the ROI. The left column corresponds to the reconstruction computed using both data sets, whereas the right column illustrates the reconstruction obtained from the projection data only. The first row of Figure 3 depicts a (approximately) coronal slice, the second row a transversal slice, and the third row a sagittal slice. In each image, the dashed lines mark the locations of the other two slices.

4. DISCUSSION

In the experiment with the simulated phantom, it is apparent that incorporation of the panoramic data into the reconstruction process makes it possible to obtain information on the locations of the teeth along the mandible. Although the actual shapes of the teeth are not reconstructed properly, the gaps between the teeth are approximately at the right places. This observation is confirmed by the bottom right image of Figure 3, where the absorption distribution of the original phantom and of the two reconstructions are plotted along the sharp layer: The top right reconstruction oscillates in the same rhythm as the original phantom, whereas the bottom left reconstruction does not seem to resemble the original phantom in the direction of the mandible.

Let us then consider the reconstructions of the *in vitro* jaw specimen. Once again, the incorporation of the panoramic data into the reconstruction process provides information on the details along the mandible: In the coronal slice, the

gap between the two molar teeth is visible only in the left-hand reconstruction. Similarly, the transversal slice contains information on the locations of the teeth only if the panoramic data is used. Finally, in the left-hand sagittal slice even small details of the molar teeth are visible, whereas the right-hand slice contains none of these details. As in the case of the simulated phantom, the shapes of the molar teeth are not reconstructed exactly, but the locations of the teeth can be inferred from the left-hand slices of Figure 6. At the same time it should be emphasized that the incorporation of the panoramic data does not seem to result in the loss of any useful information.

We conclude that the crucial anatomical features can be seen in the reconstructions from projection data only, and that the locations along the dental arc are more reliably visible in the reconstructions from hybrid data. In brief, a digital panoramic device can perform as the sole tool of an implantologist for three-dimensional X-ray imaging.

5. ACKNOWLEDGEMENTS

The research project was supported by PaloDEX Group and the Finnish Technology Agency (TEKES projects 2844/31/02 and 1107/401/00) and the Academy of Finland (Finnish Programme for Centres of Excellence in Research 2006-2011).

REFERENCES

- [1] Cederlund A, Kalke M and Welander U Volumetric tomography — a new tomographic technique for panoramic units *In review*
- [2] Kelley C T 1999 *Iterative methods for optimization* (Philadelphia: SIAM)

- [3] Kolehmainen V, Vanne A, Siltanen S, Järvenpää S, Kaipio J P, Lassas M and Kalke M 2007 Bayesian inversion method for 3D dental X-ray imaging *Elektrotechnik & Informationstechnik* **124** 248-253
- [4] Kolehmainen V, Siltanen S, Järvenpää, S, Kaipio J P, Koistinen P, Lassas M, Pirttilä J and Somersalo E 2003 Statistical inversion for medical x-ray tomography with few radiographs: II. Application to dental radiology *Phys. Med. Biol.* **48** 1465–90
- [5] Natterer F 1986 *The Mathematics of Computerized Tomography* (Chichester: John Wiley & Sons, and Stuttgart: B. G. Teubner)
- [6] Siltanen S, Kolehmainen V, Järvenpää S, Kaipio J P, Koistinen J, Lassas M, Pirttilä J and Somersalo E 2003 Statistical inversion for medical x-ray tomography with few radiographs: I. General theory *Phys. Med. Biol.* **48** 1437–63
- [7] Tikhonov A N 1963 Solution of incorrectly formulated problems and the regularization method *Soviet Mathematics — Doklady* **4** 1035–38

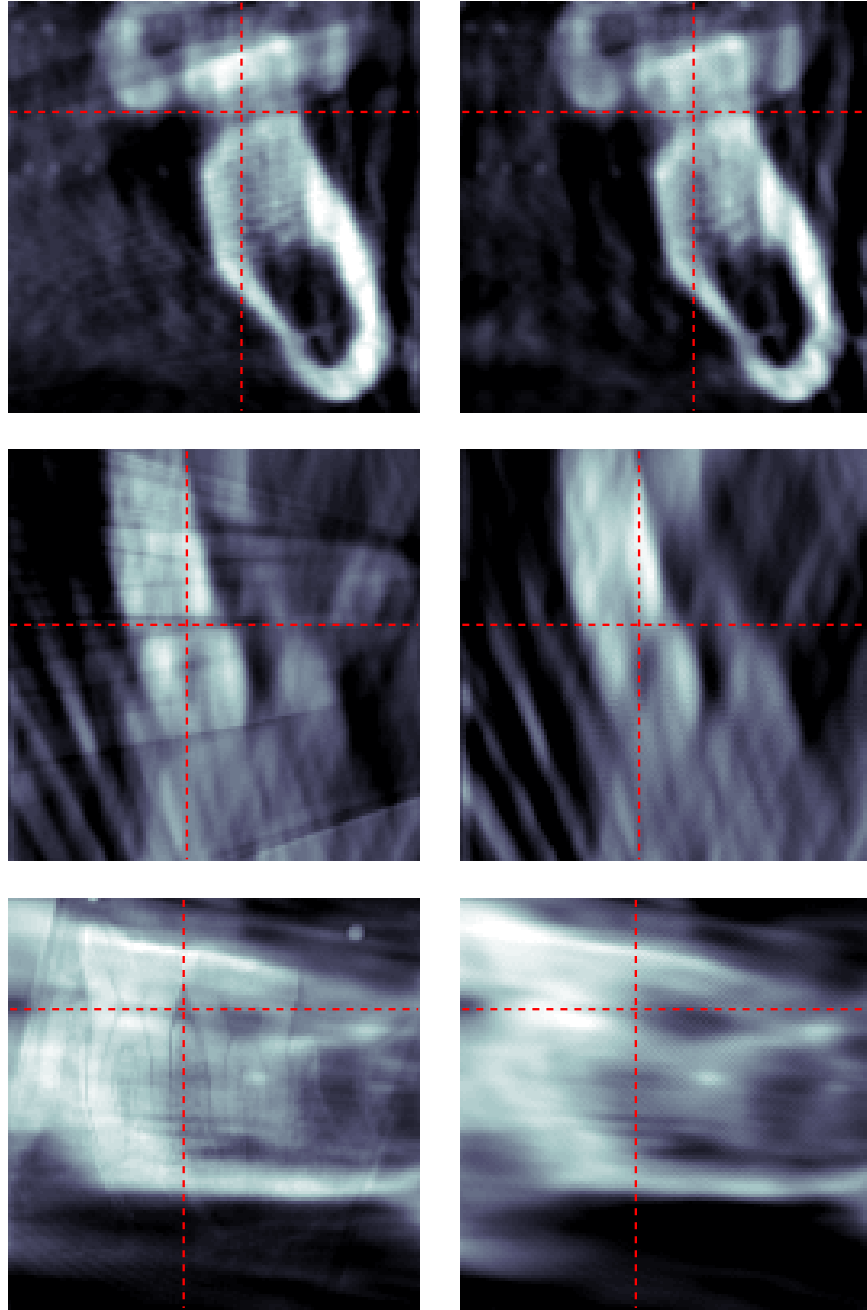


FIGURE 6. The reconstructions of the *in vitro* jaw specimen. The left column illustrates the reconstruction from both data sets, and the right column the one from the projection data only. Top: a coronal slice. Middle: a transversal slice. Bottom: a sagittal slice. The dashed lines mark the locations of the other two slices.